Modelling crack propagation using a non-matching SBFEM-FEM coupled method

X.F Wang[1], *Z.J Yang[1,2] and D.S Yin[3]

[1]School of Mechanical, Aerospace and Civil Engineering, the University of Manchester, Manchester, L13 9PL, UK
[2]College of Civil Engineering and Architecture, Zhejiang University, Hangzhou, 310058, China
[3]College of Hydraulic and Environmental Engineering, Three Gorges University, Yichang, 443002, China

*Corresponding author: zhjyang@zju.edu.cn

Abstract

A method coupling the scaled boundary finite element method (SBFEM) and the finite element method (FEM) is developed for linear elastic fracture modelling. A very simple but effective remeshing procedure based on the finite element mesh only is used to accommodate crack propagation. The crack-tip region is modelled by one SBFE subdomain whose semi-analytical displacement solutions are used to extract accurate stress intensity factors. The SBFE subdomain boundary is coupled with the surrounding FE mesh boundary through virtual interfaces so that the nodal discretisations of the two boundaries can be different. Two plane problems are modelled to validate the new method.

Keywords: scaled boundary finite element method, non-matching mesh, stress intensity factors, crack propagation, remeshing procedure, linear elastic fracture mechanics.

1. Introduction

The FEM is the most popular numerical method in simulating crack propagation because of the high generality and flexibility of finite elements in modelling structures with complex geometries, various boundaries and loading conditions, and complicated cracking patterns. The scaled boundary finite element method (SBFEM) (Song and Wolf 1997) is a semi-analytical method that is very efficient in modelling problems with discontinuities and singularities. This study proposes a non-matching SBFEM-FEM coupled method to simulate crack propagation problems based on the linear elastic fracture mechanics (LEFM). In this method, the SBFE subdomain boundary is coupled with the surrounding FE mesh boundary through virtual interfaces so that the nodal discretisations of the two boundaries can be different and only one SBFE subdomain is needed at a crack tip.

2. The Non-matching SBFEM-FEM Coupled method

2.1. The Scaled Boundary Finite Element Method

Fig. 1 illustrates a two-dimensional (2D) SBFEM subdomain. The normalised radial coordinate ξ and circumferential coordinate s form a local coordinate system used in the subdomain. They are related to the Cartesian coordinates (x, y) by the transformation Eqs. (Song and Wolf 1997)

$$x = x_0 + \xi x_s(s) \qquad y = y_0 + \xi y_s(s) \tag{1}$$

The displacement vector at any point (ξ, s) in a subdomain can be calculated as

$$\mathbf{u}(\xi, s) = \mathbf{N}_b(\xi, s)\mathbf{u}_b \tag{2}$$

where $\mathbf{u}_b$ is the nodal displacement vector of the subdomain, and the shape function matrix $\mathbf{N}_b$ is (Deeks and Wolf 2002)

$$\mathbf{N}_b(\xi, s) = \mathbf{N}_b(s)\mathbf{\Phi}\left[\xi^{\lambda}\right]\mathbf{\Phi}^{-1} \tag{3}$$

where $\mathbf{N}_b(s)$ is the one-dimensional shape function matrix as in FEM, $[\lambda] = \mathrm{diag}(\lambda_1, \lambda_2, ..., \lambda_n)$ and $\mathbf{\Phi} = \{\boldsymbol{\varphi}_1, \boldsymbol{\varphi}_2, \ldots, \boldsymbol{\varphi}_n\}$ are the subset of positive eigenvalues and modal displacements obtained from

solving an eigenvalue problem (Deeks and Wolf 2002), and n is the degrees of freedom (DOFs) of the subdomain.

The stress field $\boldsymbol{\sigma}(\xi, s)$ in a subdomain is

$$\boldsymbol{\sigma}(\xi, s) = \mathbf{DB^1}(s)\left[\sum_{i=1}^{n} c_i \lambda_i \xi^{(\lambda_i - 1)} \boldsymbol{\varphi}_i\right] + \mathbf{DB^2}(s)\left[\sum_{i=1}^{n} c_i \xi^{(\lambda_i - 1)} \boldsymbol{\varphi}_i\right] \tag{4}$$

where c_i are constants dependent on boundary conditions, $\mathbf{D}$ is the elastic matrix, and $\mathbf{B}^1(s)$ and $\mathbf{B}^2(s)$ are strain-displacement matrices (Deeks and Wolf 2002).

The stiffness matrix of the subdomain with respect to the boundary DOFs is

$$\mathbf{K_b} = \mathbf{E^0}\boldsymbol{\Phi}[\lambda]\boldsymbol{\Phi}^{-1} + \mathbf{E^{1}}^{T} \tag{5}$$

where $\mathbf{E^0}$ and $\mathbf{E^1}$ are matrices dependent on the geometry and material properties of the subdomain only.

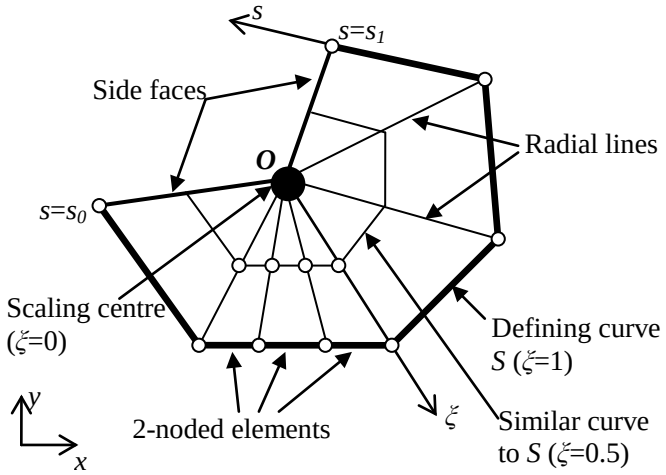

Fig. 1. A subdomain in SBFEM

2.2. Coupling SBFEM and FEM with non-matching meshes

Fig. 2a shows a domain Ω with a crack, modelled by a FE part Ω_{FE} away from the crack tip and an SBFE subdomain Ω_{SB} surrounding the crack tip. Fig. 2b shows the virtual interface of zero in-plane thickness (the dashed line), which coincides with the defining curve S (with ξ=1) of the SBFE subdomain Ω_{SB}.

For any point with circumferential coordinate s on the virtual interface S, there is a point *1* on the FE boundary and a point *2* on the SBFE boundary, possessing the same coordinates (plotted as white triangles in Fig. 2b). The displacement vector $\mathbf{d}_1(s)$ of point *1* in the global coordinate system can be calculated by

$$\mathbf{d}_1(s) = \mathbf{N}_f(s)\mathbf{u}_f \tag{6}$$

where $\mathbf{u}_f$ is the nodal displacement vector of the finite element f in which the point *1* is located, and $\mathbf{N}_f(s)$ is the shape function matrix at point *1* in the finite element f, whose members are functions of the two local parametric coordinates of point *1* in the finite element f. The displacement vector $\mathbf{d}_2(s)$ of point *2* can be calculated by Eq. (2) as

$$\mathbf{d}_2(s) = \mathbf{N}_b(s)\mathbf{u}_b \tag{7}$$

where $\mathbf{N}_b(s)$ are functions of circumferential coordinate s only as ξ=1 on the defining curve S.

To simplify derivation, Eqs. (6) and (7) can be rewritten by expanding $\mathbf{u}_f$, $\mathbf{u}_b$, $\mathbf{N}_f(s)$ and $\mathbf{N}_b(s)$ to the global DOFs as

$$\mathbf{d}_1(s) = \mathbf{N}_1(s)\mathbf{u} \tag{8}$$

$$\mathbf{d}_2(s) = \mathbf{N}_2(s)\mathbf{u} \tag{9}$$

where **u** is the nodal displacement vector of the whole model with N number of DOFs, and $\mathbf{N}_1(s)$ and $\mathbf{N}_2(s)$ are now both $2\times N$ matrices.

The relative displacements of points *1* and *2*, with one component along the virtual interface and another normal to it, are

$$\bar{\mathbf{d}}(s) = \mathbf{L}(s)(\mathbf{d}_1(s) - \mathbf{d}_2(s)) \tag{10}$$

where

$$\mathbf{L}(s) = \begin{bmatrix} cos\theta(s) & -sin\theta(s) \\ sin\theta(s) & cos\theta(s) \end{bmatrix} \tag{11}$$

is the coordinate transformation matrix and $\theta(s)$ is the inclination angle of the virtual interface at the point and measured clockwise from s direction to the positive x axis (see Fig. 2b).

Assuming that the relative displacements are sustained by two virtual springs with stiffness coefficients k_s along the virtual interface and k_n normal to it, the force vector on unit length transferred by the springs is

$$\mathbf{P}(s) = \mathbf{D}_c\bar{\mathbf{d}}(s) \tag{12}$$

with

$$\mathbf{D}_c = \begin{bmatrix} k_s & \\ & k_n \end{bmatrix} \tag{13}$$

The introduction of the virtual interface and the virtual springs leads to artificial gaps or penetrations along the shared boundary, and spurious potential energy which should be minimised. The potential energy on the whole virtual interface is

$$\Pi = \int_S \frac{1}{2}\mathbf{P}(s)\bar{\mathbf{d}}(s)ds \tag{14}$$

Substituting Eqs. (10) to (12) into Eq. (14) and using Eqs. (8) and (9) results in

$$\Pi = \int_S \frac{1}{2}\bar{\mathbf{d}}(s)^{\mathrm{T}}\mathbf{D}_c\bar{\mathbf{d}}(s)ds = \frac{1}{2}\int_S \mathbf{u}^{\mathrm{T}}(\mathbf{N}_1{}^{\mathrm{T}}(s) - \mathbf{N}_2{}^{\mathrm{T}}(s))\mathbf{L}(s)^{\mathrm{T}}\mathbf{D}_c\mathbf{L}(s)(\mathbf{N}_1(s) - \mathbf{N}_2(s))\mathbf{u}ds \tag{15}$$

Calculating variation of Eq. (15) with respect to **u** leads to

$$\delta\Pi = \delta\mathbf{u}^{\mathrm{T}}\int_S \left[\mathbf{N}_1{}^{\mathrm{T}}(s)\bar{\mathbf{D}}_c(s)\mathbf{N}_1(s) + \mathbf{N}_2{}^{\mathrm{T}}(s)\bar{\mathbf{D}}_c(s)\mathbf{N}_2(s) - \mathbf{N}_1{}^{\mathrm{T}}(s)\bar{\mathbf{D}}_c(s)\mathbf{N}_2(s) - \mathbf{N}_2{}^{\mathrm{T}}(s)\bar{\mathbf{D}}_c(s)\mathbf{N}_1(s)\right]ds\cdot\mathbf{u} \tag{16}$$

where

$$\bar{\mathbf{D}}_c(s) = \mathbf{L}(s)^{\mathrm{T}}\mathbf{D}_c\mathbf{L}(s) \tag{17}$$

Thus the contribution of the virtual interface to the system stiffness matrix is (Zienkiewicz et al. 2005)

$$\mathbf{K_c} = \int_S \left[\mathbf{N}_1{}^{\mathrm{T}}(s)\bar{\mathbf{D}}_c\mathbf{N}_1(s) + \mathbf{N}_2{}^{\mathrm{T}}(s)\bar{\mathbf{D}}_c(s)\mathbf{N}_2(s) - \mathbf{N}_1{}^{\mathrm{T}}(s)\bar{\mathbf{D}}_c(s)\mathbf{N}_2(s) - \mathbf{N}_2{}^{\mathrm{T}}(s)\bar{\mathbf{D}}_c(s)\mathbf{N}_1(s)\right]ds \tag{18}$$

The system stiffness matrix is then obtained by assembling Eq. (5), Eq. (18) and the stiffness matrices of all the finite elements.

The spring stiffness coefficients k_s and k_n play a vital role in the accuracy of this coupling procedure. Too high values may lead to ill-posedness of the system equations and too low values cannot ensure displacement continuity across the virtual interface. The following is proposed in (Qiang et al. 2000) as a guideline

$$k_s = k_n = k = \frac{c(1-v)}{b(1+v)(1-2v)}E \tag{19}$$

where E and v are the Young's modulus and Poisson's ratio, b is the characteristic size of elements, and c is taken as 10~100 from the experience in (Qiang et al. 2000) .

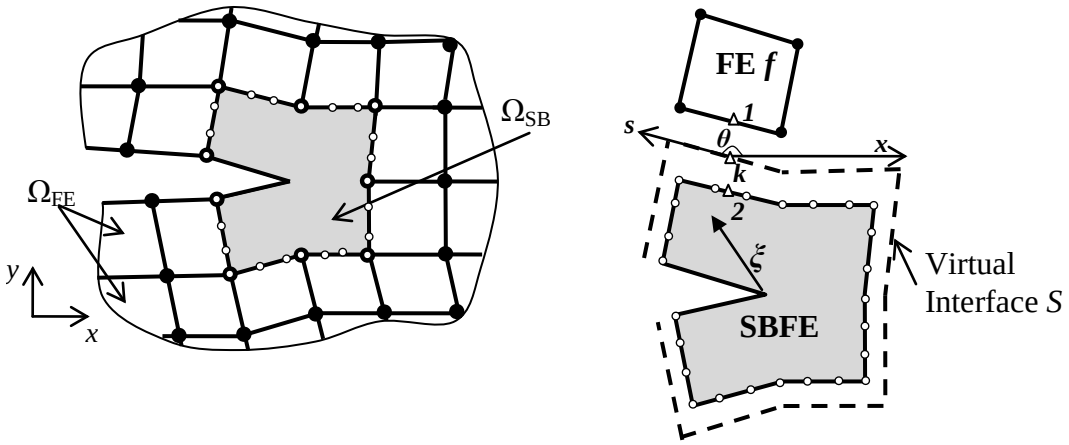

(a) The global mesh (b) The local mesh

Fig. 2. Coupling SBFE and FE meshes

3. Numerical examples

When a crack is judged to propagate, a very simple, local remeshing procedure similar to the one in (Xie and Gerstle 1995) is used to accommodate its propagation. The crack propagation direction is calculated by the maximum circumferential stress theory in this study (Erdogan and Sih 1963). The SIFs are extracted directly from the displacement solutions (Chidgzey and Deeks 2005). Two problems are modelled to validate the developed method and demonstrate its capability.

3.1. An edge-cracked plate under mode-I fracture

The first example is an edge-cracked plate subjected to a far field unit stress (σ=1) applied on the top and bottom. The geometry, boundary and loading conditions are shown in Fig. 3a. The exact solution of the mode-I SIF in this example is K_{Ie}= 9.37 (Ingraffea et al. 1984).

To investigate the effects of the coupling parameter k in Eq. (19), structured FE meshes are modelled. Fig. 3b shows a mesh with 20×40 4-noded quadrilateral elements. The FE-SBFE coupled mesh is shown in Fig. 3c, with the detailed region at the crack tip highlighted in Fig. 3d.

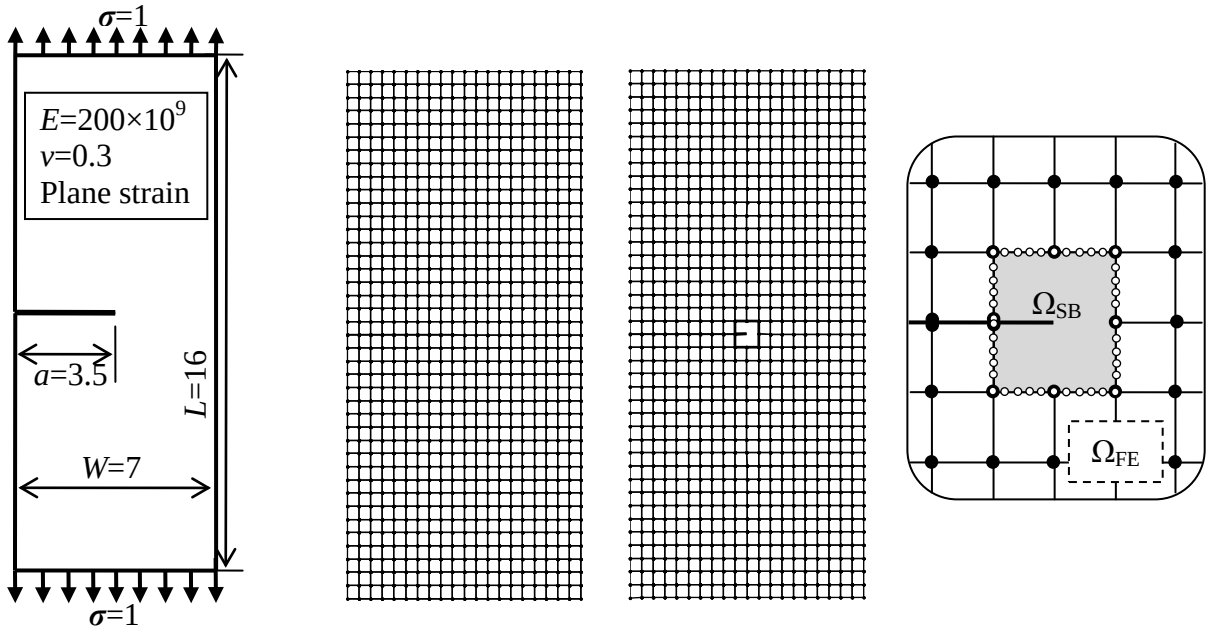

(a) Geometry and loading conditions **(b) FE mesh** **(c) FE-SBFE coupled mesh** **(d) detailed mesh at the crack-tip**

Fig. 3. Example 1: a plate with an edge crack

Fig. 4 plots the errors of K_I from three meshes as the virtual spring stiffness coefficient k varies. It is reconfirmed that too high or too low values of k lead to unsatisfactory accuracy. For this example, it is found that k=10^2E~$10^{10}E$ results in lower than 1% error in K_I. From the vertical displacement contours shown in Fig. 5 (20×40 mesh), the use of virtual interface between the FE and SBFE meshes does not affect the displacement continuity. k=100E is used in all the following examples, corresponding to c=26 in Eq. (19).

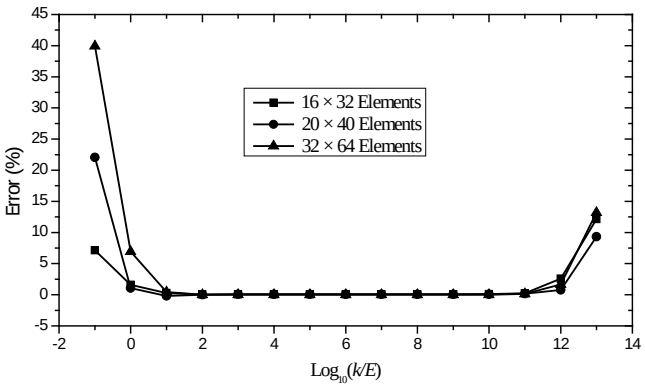

Fig. 4. Effects of virtual spring stiffness coefficient k on K_I

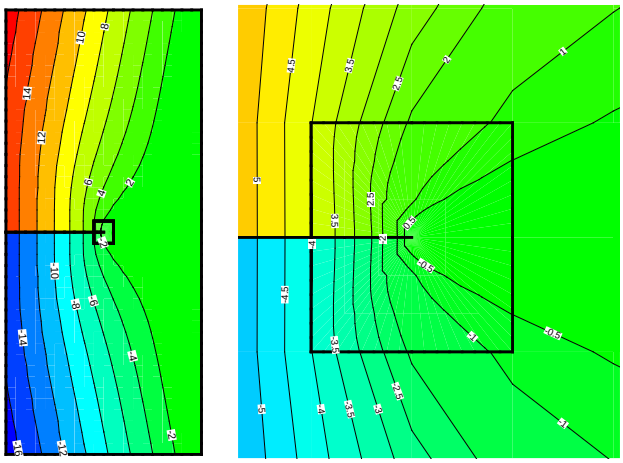

(a) Global **(b) Local at crack tip**

Fig. 5. Vertical displacement contours from structured 20×40 mesh (×10^{-11})

Table 1 compares the relative error of K_I for five structured meshes using the FEM, the XFEM, the hybrid FE-SBFE method (Ooi and Yang 2010) and the present method. The results are also shown in Fig. 6, which indicate the much higher accuracy of the present method and the previous FE-SBFE hybrid method (Ooi and Yang 2010) over FEM and XFEM.

Table 1. Errors of K_I for the edge-cracked plate under mode-I loading

FEM			XFEM (Ooi and Yang 2010)			Hybrid method (Ooi and Yang 2010)			Present method		
No. Elements	No. DOF	Error (K_I)	No. Elements	No. DOF	Error (K_I)	No. Elements	No. DOF	Error (K_I)	No. Elements	No. DOF	Error (K_I)
4 × 8	94	25.0%	5 × 7	136	18.5%	4 × 8	222	7.4%	4 × 8	222	7.2%
8 × 16	314	14.3%	9 × 15	368	8.4%	8 × 16	442	3.5%	8 × 16	442	3.6%
16 × 32	1138	7.6%	17 × 31	1216	3.7%	16 × 32	1266	1.4%	16 × 32	1266	1.7%
20 × 40	1742	4.2%	21 × 39	1832	2.9%	20 × 40	1870	1.0%	20 × 40	1870	1.3%
32 × 64	4322	4.0%	33 × 63	4448	1.7%	32 × 64	4450	0.5%	32 × 64	4450	0.8%

The influence of the number of DOFs used to model the SBFE subdomain is shown in Fig. 7. It can be seen that using 30 nodes can achieve less than 1% error (32×64 elements).

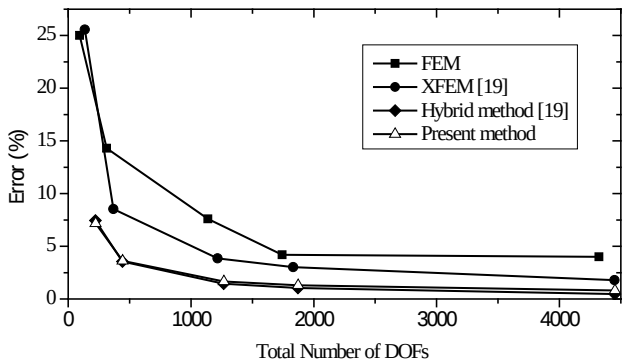

Fig. 6. Effects of total DOFs

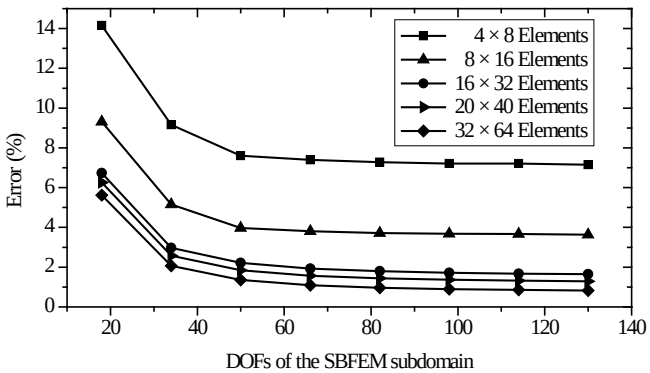

Fig. 7. Effects of DOFs of the SBFE subdomain

3.2. A double-edge notched plate with two holes

The second example is a plate with two holes and two edge cracks subjected to a uniform tensile test, shown in Fig. **8**. Fig. **9** and Fig. **10** show two final FE-SBFE coupled meshes, with 1722 and 6208 DOFs, respectively. The predicted crack paths using the two meshes are very close. Fig. 11 compares the crack paths predicted by the present method with those obtained by the FEM in (Bouchard et al. 2003) and the polygon SBFEM in (Ooi et al. 2012).

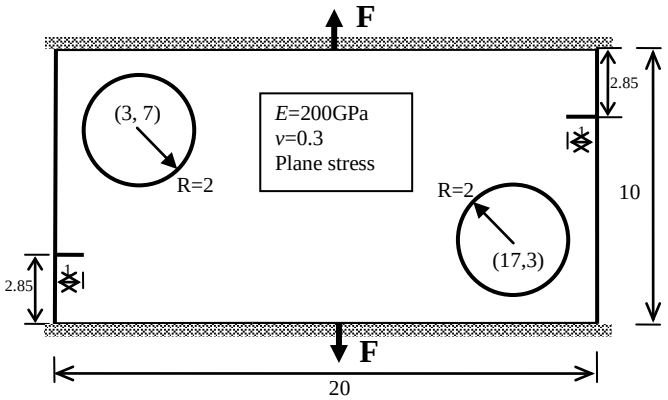

Fig. 8. A plate with two holes and two edge cracks (unit: mm)

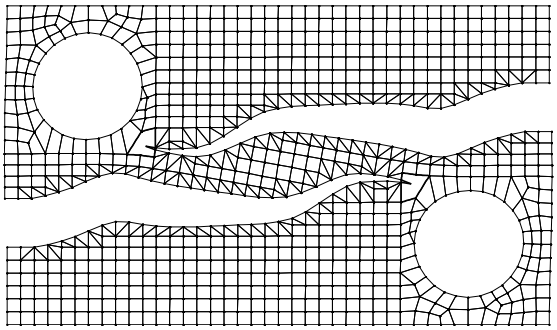

Fig. 9. Mesh 1, 772 finite elements, 861 nodes (displacement scale=50)

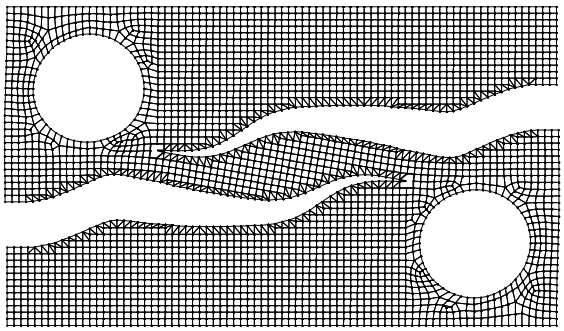

Fig. 10. Mesh 1, 772 finite elements, 861 nodes (displacement scale=50)

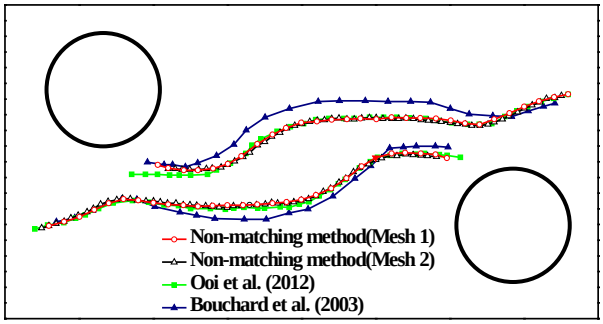

Fig. 11. Comparison of crack paths

4. Conclusions

A non-matching SBFEM-FEM coupled method has been developed for modelling LEFM-based crack propagation. The stress singularities are accurately captured by crack-tip SBFE subdomains, making the FE-based remeshing procedure as simple as possible. The use of non-matching FE and SBFE meshes, whose displacement continuity is ensured by assigning sufficiently high stiffness on the virtual interface, makes remeshing even more flexible than other methods. The accuracy and effectiveness of the developed method has been demonstrated by modelling two fracture problems. It also paves the way for further development, such as the overlapping methods (Massing et al. 2012; Okada et al. 2005) in which the cracked subdomain floats on the global FE mesh, namely, the two meshes are completely independent. This will offer the highest flexibility in remeshing.

5. Acknowledgement

XF Wang is funded by an EPS Faculty PhD Studentship from the University of Manchester, UK. ZJ Yang would like to thank the Alexander von Humboldt Foundation, Germany for a Fellowship for Experienced Researchers. The discussion with Dr ET Ooi at the University of New South Wales is highly appreciated.

References

Bouchard, P.-O., F. Bay & Y. Chastel (2003), Numerical modelling of crack propagation: automatic remeshing and comparison of different criteria. *Computer methods in applied mechanics and engineering,* 192**,** 3887-3908.

Chidgzey, S. R. & A. J. Deeks (2005), Determination of coefficients of crack tip asymptotic fields using the scaled boundary finite element method. *Engineering fracture mechanics,* 72**,** 2019-2036.

Deeks, A. J. & J. P. Wolf (2002), A virtual work derivation of the scaled boundary finite-element method for elastostatics. *Computational Mechanics,* 28**,** 489-504.

Erdogan, F. & G. Sih (1963), On the crack extension in plates under plane loading and transverse shear. *Journal of basic engineering,* 85**,** 519.

Ingraffea, A. R., W. H. Gerstk, P. Gergely & V. Saouma (1984), Fracture mechanics of bond in reinforced concrete. *Journal of Structural Engineering,* 110**,** 871-890.

Massing, A., M. G. Larson & A. Logg (2012), Efficient implementation of finite element methods on non-matching and overlapping meshes in 3D. *arXiv preprint arXiv:1210.7076*.

Okada, H., S. Endoh & M. Kikuchi (2005), On fracture analysis using an element overlay technique. *Engineering Fracture Mechanics,* 72**,** 773-789.

Ooi, E. T., C. M. Song, F. Tin-Loi & Z. J. Yang (2012), Polygon scaled boundary finite elements for crack propagation modelling. *International Journal for Numerical Methods in Engineering,* 91**,** 319-342.

Ooi, E. T. & Z. J. Yang (2010), A hybrid finite element-scaled boundary finite element method for crack propagation modelling. *Computer Methods in Applied Mechanics and Engineering,* 199**,** 1178-1192.

Qiang, T. C., X. D. Kou & W. Y. Zhou (2000), Three-dimensional FEM Interface Coupled Method and its Application to Arch Dam Fracture Analysis. *Chinese Journal of Rock Mechanics and Eng ineering,* 19**,** 562-566.

Song, C. M. & J. P. Wolf (1997), The scaled boundary finite-element method—alias consistent infinitesimal finite-element cell method—for elastodynamics. *Computer Methods in Applied Mechanics and Engineering,* 147**,** 329-355.

Xie, M. & W. H. Gerstle (1995), Energy-based cohesive crack propagation modeling. *Journal of engineering mechanics,* 121**,** 1349-1358.

Zienkiewicz, O. C., R. L. Taylor & J. Z. Zhu(2005), The finite element method: its basis and fundamentals. *Butterworth-Heinemann*, Oxford.